Modelling laser induced melting

Modelling laser induced melting

J.C.J. Verhoeven, J.K.M. Jansen, R.M.M. Mattheij, W.R. Smith

Department of Mathematics and Computing Science, Eindhoven University of Technology, P.O. Box 513, 5600 MB Eindhoven, The Netherlands

Abstract

In simulating a laser drilling process, melting is one of several physical phenomenae that have to be modelled. Two different mathematical formulations of this laser induced melting are derived. For every formulation we give a specific numerical recipe. Special attention is paid to problems where 'mushy regions' occur and to extension to 2D. Finally, the numerical results of these different recipes are discussed.

1 Introduction

Lasers are often used to machine materials when conventional techniques fail. Laser percussion drilling is one of these applications. For instance, this drilling technique is used to drill cooling holes in fans, which are part of a gas turbine; such fans are typically made of super alloys. The term "percussion" refers to the repeated operation of the laser in short pulses (10^{-3} s), which are separated by longer time periods (10^{-2} s). The energy supplied by the laser is bounded and pulsewise behaviour allows for large bursts of energy. These energy bursts cause local melting and splashing of material and sometimes (unwanted) local recasting. The finer details of the laser percussion drilling process is not yet fully understood. To get a better understanding of the process, a mathematical model is needed. Because of the (known) importance of molten material to the process a melting model has to be incorporated into this model.

We shall first sketch the physical process in order to indicate where this melting model comes into play. A laser percussion drilling process may in fact be split up into three stages. Initially, a thin region of molten material is formed by absorption of laser energy at the target surface. After some time, the surface of this melt pool reaches vaporisation temperature. The sudden expansion of the vapour evaporating from the surface leads to the final stage: the meltpool is being pushed out by the recoil pressure. On its way out some part of this molten material may resolidify at the walls. Thus, during these three stages three events occur for which a melting model is needed. These events are depicted in Figure 1. A simple melting model can be used to predict the precise dimensions of the melt pool, as generated by the incoming radiation, see Fig 1(a). More sophisticated models are needed to deal with splashing (Fig 1(b)) and with solidification (Fig 1(c)). In fact, we can show that a one-dimensional melting model applies for the initial stage. This itself is sufficiently interesting to investigate in detail, and we shall therefore concentrate on 1-D modelling and only briefly use 2-D computations to validate this. Yet, for splashing and solidification more complicated models will be needed. We hope to report on these in a subsequent paper.

Melting problems are commonly known as *Stefan problems* named after J. Stefan, who wrote his famous article about the building up of ice in polar seas in 1891, see [9]. Several formulations of melting problems have been studied in literature so far; extensive overviews can be found in [2, 3, 13]. In this paper we will focus on the formulation using the original Stefan condition (see e.g. [1]) and the enthalpy method (see for instance [10, 11, 12]). Furthermore, we will pay attention to finding suitable initial conditions for the formulation using the Stefan condition in applying this method to the laser percussion drilling process. To be able to deal with superalloys in the splashing and solidification models, we will assess the problems both for materials having a melting range and for materials with a discrete melting point.

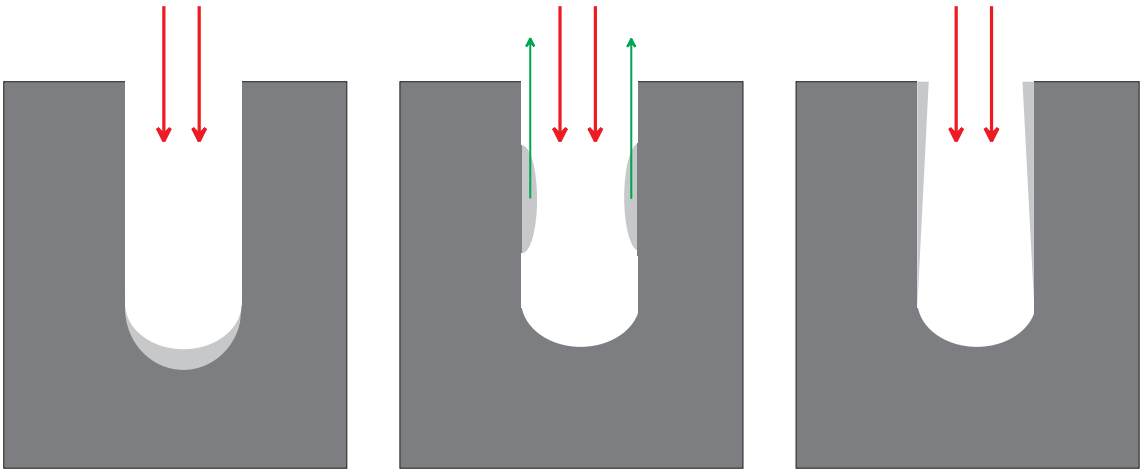

(a) Formation of a melt pool

(b) Squirting out of molten material

(c) Resolidified material, the so called *recast* layer

Figure 1: *The three events in a laser percussion drilling process where a melting model is needed: (a) melting, (b) splashing and (c) resolidification.*

The setup of this article is as follows. In Section 2 we will show that it is reasonable (at least for the initial stage of our process) to employ a one-dimensional model. Two formulations of a one-dimensional melting model will then be the subject of Section 3. The numerical methods related to these two different formulations will be studied in Section 4. In Section 5 the extension to two spatial dimensions will be studied for both formulations. Numerical results of the models will be presented and discussed in Section 6. Finally, the conclusions of this work will be given in Section 7.

2 Mathematical modelling

The lasers used in pratice to drill holes typically produce a Gaussian intensity distribution, which is, ideally, axisymmetric. Moreover, further examination shows that radial diffusion is negligable, which can be seen as follows: take an axi-symmetric coordinate system, where $z = 0$ denotes the surface of the irradiated material, see Figure 2. The density ρ, the specific heat capacity c and the

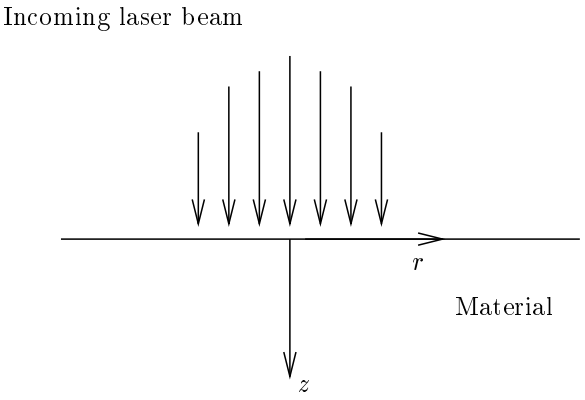

Figure 2: *Geometry of the model.*

Symbol	Definition	Value
ρ	density	2.7×10^3 kg m $^{-3}$
L_f	latent heat of fusion	3.6×10^5J kg^{-1}
k	thermal conductivity	2.3×10^2 W m^{-1}K^{-1}
c	specific heat capacity	9.0×10^2 J kg^{-1}K^{-1}
T_m	melting temperature	9.3×10^2K
T_v	vaporisation temperature	2.5×10^3 K

Table 1: *Physical data for drilling aluminium.*

Symbol	Definition	Value
I_{ref}	energy input	1.5×10^{10} W m^{-2}
w_0	waist	1×10^{-3} m

Table 2: *Physical data for the laser beam.*

thermal conductivity k of the material are known and assumed to be constant. The temperature T in the material is governed by the heat equation in cylindrical coordinates, which, employing the axisymmetry, is given by

$$\rho c \frac{\partial T}{\partial t} = \frac{k}{r}\frac{\partial}{\partial r}\left(r\frac{\partial T}{\partial r}\right) + k\frac{\partial^2 T}{\partial z^2}. \tag{2.1}$$

The intensity distribution of the laser beam is given by $I = I(r,t)$. The laser energy is supplied at the surface $z = 0$, yielding

$$k\frac{\partial T}{\partial z} = -I. \tag{2.2}$$

Before nondimensionalising we introduce some typical numbers. For the temperature we need the vaporisation temperature T_v and the melting temperature T_m. (In Table 1 we give typical parameters for aluminium.) For the radial coordinate the *waist*, denoted by w_0, of the (Gaussian) laser beam is used as a typical length scale. Furthermore, let I_{ref} be a typical intensity. Some data for a Nd:YAG laser used in drilling can be found in Table 2. From this we can define the dimensionless variables (indicated by a superbar) by

$$z =: \frac{k(T_v - T_m)}{I_{ref}}\bar{z}, \tag{2.3}$$

$$r =: w_0\bar{r}, \tag{2.4}$$

$$t =: \frac{\rho c k (T_v - T_m)^2}{I_{ref}^2}\bar{t}, \tag{2.5}$$

$$T =: T_m + (T_v - T_m)\bar{T}. \tag{2.6}$$

The dimensionless length scale in z-direction comes from balancing the two terms in the boundary condition (2.2). The dimensionless time scale $\bar{t}$ as introduced in (2.5) is the corresponding diffusive time scale, as follows from (2.1). Writing (2.1) together with the influx of energy (2.2) in dimensionless form we obtain

$$\frac{\partial \bar{T}}{\partial \bar{t}} = \varepsilon\frac{1}{\bar{r}}\frac{\partial}{\partial \bar{r}}\left(\bar{r}\frac{\partial \bar{T}}{\partial \bar{r}}\right) + \frac{\partial^2 \bar{T}}{\partial \bar{z}^2}, \tag{2.7}$$

Symbol	Definition	Value
ε	$k^2(T_v - T_m)^2/(w_0^2 I_{ref}^2)$	6.1×10^{-4}
T_a	$(T_a - T_m)/(T_v - T_m)$	-0.4
λ_f	$L_f/c(T_v - T_m)$	0.25

Table 3: *Dimensionless parameters for typical laser percussion drilling processes in aluminium.*

where

$$\varepsilon = \frac{k^2(T_v - T_m)^2}{w_0^2 I_{ref}^2}, \tag{2.8}$$

and

$$\frac{\partial \bar{T}}{\partial \bar{z}} = -\frac{I}{I_{ref}}, \qquad \bar{z} = 0. \tag{2.9}$$

For typical laser percussion drilling parameters, $\varepsilon \ll 1$, see Table 3. Thus, radial diffusion can be neglected on the typical scales and our model for the initial stage of the laser percussion drilling process degenerates to a one-dimensional model. This one-dimensional model will therefore be studied in the remainder of this paper and we will only use results of 2-D computations to validate this.

In order to melt a material an extra amount of energy is needed on top of the amount needed to raise the temperature. This energy is called the latent heat of fusion L_f. Typical values of this quantity for aluminium can be found in Table 1.

3 Mathematical Formulations of Melting

In this section we will outline two different ways to formulate the melting problem. Each formulation will give rise to a numerical scheme with its own vices and virtues. As shown in the previous section the importance of radial diffusion in laser induced melting is negligible. Therefore, we will study the one-dimensional model.

We shall consider two models. One is based on use of the Stefan condition; this will therefore be referred to as the *Stefan problem*. The other is employing an enthalpy formulation, and will be referred to as the *enthalpy problem*.

3.1 The Stefan Problem

Let Ω_l denote the liquid region $0 \leq z < s(t)$ and Ω_s the solid region $s(t) < z < \infty$. Furthermore, let $s(t)$ be the position of the solid-liquid interface. The geometry is sketched in Figure 3. The temperature in both the liquid and the solid region is governed by the heat equation,which in dimensionless form reads

$$\frac{\partial T_i}{\partial t} = \frac{\partial^2 T_i}{\partial z^2} \quad \text{in } \Omega_i \qquad \text{for } i = s, l. \tag{3.1}$$

Here the subscripts s and l refer to solid and liquid, respectively. At the boundary $z = 0$ the laser supplies an intensity $I = I(r, t)$,

$$\frac{\partial T_l}{\partial z} = -\frac{I}{I_{ref}}, \qquad z = 0. \tag{3.2}$$

For a material to melt, an extra amount of energy has to be supplied, the *latent heat of fusion*, which, in dimensionless form, is defined as

$$\lambda_f := \frac{L_f}{c(T_v - T_m)}. \tag{3.3}$$

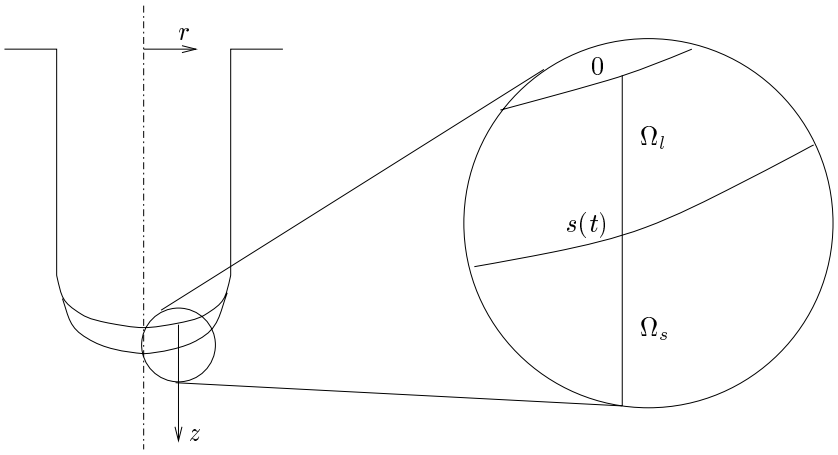

Figure 3: *The geometry of the laser induced melting problem.*

At the solid-liquid interface we need an equation that expresses this absorption of heat needed for phase change. This equation is commonly known as the *Stefan condition* and is given by

$$\left.\frac{\partial T_l}{\partial z}\right|_{z\uparrow s} - \left.\frac{\partial T_s}{\partial z}\right|_{z\downarrow s} = -\lambda_f \frac{ds}{dt}, \qquad z = s(t). \tag{3.4}$$

Moreover, the temperature is assumed to be continuous across the interface

$$T_s = T_l = 0 \qquad z = s(t). \tag{3.5}$$

At infinity, the boundary condition

$$T_s \to T_a, \qquad z \to \infty \tag{3.6}$$

holds, where T_a is the dimensionless ambient temperature of the material. We start with a known temperature distribution

$$T(z,0) = T_0(z). \tag{3.7}$$

3.2 The Enthalpy Problem

The enthalpy H is defined as the sum of the sensible and the latent heat in a substance. If a material is liquid it contains latent heat of fusion per unit mass L_f, in addition to the sensible heat ρcT. Figure 4 shows the relation between the temperature and the enthalpy for two different materials. Figure 4(a) shows this relation for pure substances with a single melting-point temperature, whereas figure 4(b) illustrates this relation for a material where the phase change takes place over an extended temperature range from the solidus temperature T_{sol} to the liquidus temperature T_{liq}. The region with temperature between the solidus and the liquidus temperature is referred to as the *mushy region*. In order to nondimensionalise the enthalpy we introduce two typical numbers. The first is the enthalpy at vaporisation temperature H_v, which is given by

$$H_v = \rho c T_v + \rho L_f. \tag{3.8}$$

For materials with a discrete melting point the second number is the enthalpy at melting temperature H_m, given by

$$H_m = \rho c T_m, \tag{3.9}$$

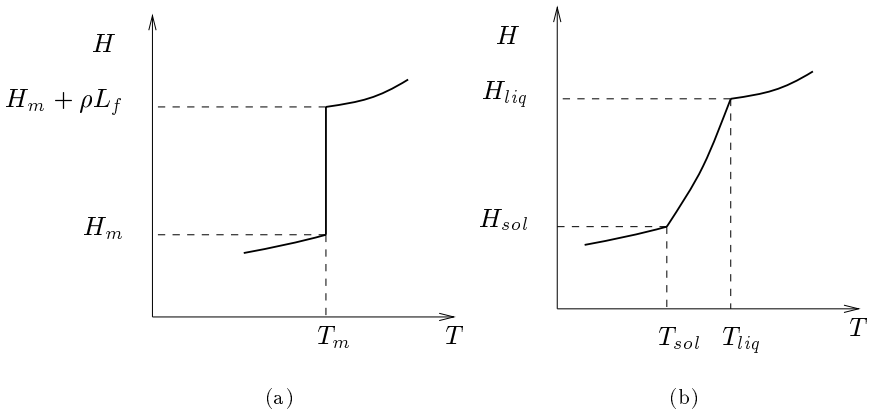

Figure 4: *Relation of enthalpy and temperature for (a) pure crystalline substances and (b) glassy substances and alloys.*

whereas for glassy substances and alloys this second number is the enthalpy at solidus temperature

$$H_{sol} = \rho c T_{sol}. \tag{3.10}$$

Hence, the dimensionless enthalpy $\bar{H}$ is for pure materials given by

$$H = H_m + (H_v - H_m)\bar{H}, \tag{3.11}$$

and by

$$H = H_{sol} + (H_v - H_{sol})\bar{H}, \tag{3.12}$$

for materials with a melting range. For later use we introduce the constants D_1 and D_2 by

$$D_1 := \frac{\rho c(T_v - T_m)}{H_v - H_m}, \tag{3.13a}$$

and

$$D_2 := \frac{\rho c(T_v - T_{sol})}{H_v - H_{sol}}. \tag{3.13b}$$

We will drop the bars on the dimensionless variables from now on.

The relationship between the dimensionless temperature and the dimensionless enthalpy for pure materials, is given by

$$H(T) = \begin{cases} D_1\, T & T < 0, \\ [0, D_1\lambda_f]\,, & T = 0, \\ D_1\, T + D_1\lambda_f & T > 0. \end{cases} \tag{3.14}$$

Likewise, the relationship between the dimensionless enthalpy and temperatures for materials with a melting range is given by

$$H(T) = \begin{cases} D_2\, T & T \le 0, \\ D_2\, T + D_2\lambda_f \dfrac{T}{T_{liq}} & 0 \le T \le T_{liq}, \\ D_2\, T + D_2\lambda_f & T \ge T_{liq}. \end{cases} \tag{3.15}$$

Note that T_{liq} denotes the dimensionless liquidus temperature and that $\lambda_f = \frac{L_f}{c(T_v - T_{sol})}$ now.

As has been shown in Section 2, the laser induced melting problem degenerates to a one-dimensional problem. Like in the previous subsection we take the material to be in $z \geq 0$ with the surface at $z = 0$. The enthalpy and temperature of the material in this region are governed by the energy equation in enthalpy form, which, in dimensionless form, is given by

$$\frac{\partial H}{\partial t} = D_1 \frac{\partial^2 T}{\partial z^2}, \qquad z > 0, \tag{3.16}$$

for materials with a discrete melting point. For materials with a melting range D_2 takes the role of D_1. The boundary and initial conditions are the same as in the previous subsection. The influx of energy is represented by

$$\frac{\partial T}{\partial z} = -\frac{I}{I_{ref}}, \qquad z = 0. \tag{3.17}$$

We assume an ambient temperature infinity

$$T \to T_a, \qquad z \to \infty, \tag{3.18}$$

and we begin with a known initial temperature (and hence enthalpy) distribution

$$T = T_0, \qquad t = 0. \tag{3.19}$$

4 Numerical Methods

In this section we will consider the numerical techniques used to solve the Stefan problem. These numerical methods relate to the various formulations of the melting problem we saw in the previous section. Section 4.1 deals with a discretisation of the formulation using the Stefan condition, in Section 4.3 a discretisation based on the enthalpy method is dealt with. The PDE's are numerically solved by the finite element method. The finite element method is preferred to other methods such as the finite difference method because of its versatility in dealing with complex boundaries. Though we saw that the melting problem degenerates to a one-dimensional one, the procedure used to solve the enthalpy method can easily be generalised to 2D and 3D, which will be needed for the splashing and solidification models. This procedure will be outlined in the next section.

4.1 Discretisation of the Stefan Problem

Finite element methods are a powerful tool in the solution of partial differential equations, also when moving boundaries are involved cf. [2, 5]. One way to handle such a moving boundary is to use subdomains that change with time. Another way to deal with the moving boundary is to use a transformation, see e.g. [6]. The latter method, however, is not applicable to problems where no liquid is present initially.

The derivation consists of the following steps: (i) a Galerkin formulation, (ii) a discretisation method and (iii) the solution of the resulting initial value problems with (iv) suitable initial conditions. The last step involves some subtleties in our problem and will be considered separately in the next subsection.

The problem to begin with is given in Section 2.1, but we simplify it by cutting off the domain

at $z = z_b$. The problem is then given by

$$\begin{cases} \dfrac{\partial T_l}{\partial t} = \dfrac{\partial^2 T_l}{\partial z^2}, & 0 < z < s(t) \\ \dfrac{\partial T_s}{\partial t} = \dfrac{\partial^2 T_s}{\partial z^2}. & s(t) < z < z_b \\ \dfrac{\partial T_l}{\partial z} = -\dfrac{I}{I_{ref}}, & z = 0, \\ T_l = T_s = 0; \quad \left.\dfrac{\partial T_l}{\partial z}\right|_{z\uparrow s} - \left.\dfrac{\partial T_s}{\partial z}\right|_{z\downarrow s} = -\lambda_f \dfrac{ds}{dt}, & z = s(t), \\ T_s = T_a, & z = z_b, \end{cases} \tag{4.1}$$

along with suitable initial conditions for the temperature and the position of the solid-liquid interface s.

If T_l satisfies the PDE in (4.1), then it also satisfies

$$\int_0^s \left\{ \frac{\partial T_l}{\partial t} - \frac{\partial^2 T_l}{\partial z^2} \right\} v(z,t)dz = 0, \tag{4.2a}$$

for all suitable weight functions $v(z,t)$. Likewise T_s satisfies

$$\int_s^{z_b} \left\{ \frac{\partial T_s}{\partial t} - \frac{\partial^2 T_s}{\partial z^2} \right\} w(z,t)dz = 0, \tag{4.2b}$$

for all suitable weight functions $w(z,t)$. Let the weight functions $v(z,t)$ and $w(z,t)$ satisfy $v(s,t) = w(s,t) = w(z_b,t) = 0$ for all t. Using integration by partsand the first boundary condition of (4.1), (4.2) can be rewritten as

$$\int_0^s \left\{ \frac{\partial T_l}{\partial t} v(z,t) + \frac{\partial T_l}{\partial z}\frac{\partial v}{\partial z} \right\} dz = \frac{I}{I_{ref}} v(0,t), \tag{4.3a}$$

and

$$\int_s^{z_b} \left\{ \frac{\partial T_s}{\partial t} w(z,t) + \frac{\partial T_s}{\partial z}\frac{\partial w}{\partial z} \right\} dz = 0. \tag{4.3b}$$

To solve the Galerkin form (4.3), we compute approximate solutions of the boundary and the temperature distributions. First we fix the time t and divide the domains $0 \le z \le s(t)$ and $s(t) \le z \le z_b$ into N and M equal subintervals, respectively. Next, at each node in the liquid domain

$$z_{l,j} = jh_l, \qquad j = 0, \ldots, N; \quad \text{with} \qquad h_l = h_l(t) = \frac{s(t)}{N} \tag{4.4}$$

we construct the usual hat function $\varphi_{l,j}(z,t)$. The same is done for each node in the solid part

$$z_{s,j} = s(t) + jh_s, \qquad j = 0, \ldots, M; \quad \text{with} \qquad h_s = h_s(t) = \frac{z_b - s(t)}{M} \tag{4.5}$$

where the hat functions are denoted by $\varphi_{s,j}(z,t)$. Note that in contrast with the usual basis functions used for finite element methods, these basis functions depend on time. For later use we note that

$$\frac{dz_{l,j}}{dt} = j\frac{dh_l}{dt} = \frac{j}{N}\frac{ds}{dt}, \tag{4.6}$$

and

$$\frac{dz_{s,j}}{dt} = \frac{ds}{dt} + j\frac{dh_s}{dt} = \frac{M-j}{M}\frac{ds}{dt}. \tag{4.7}$$

Next we determine approximate solutions of the forms

$$T_{h_l}(z,t) = \sum_{j=0}^{N} T_{l,j}(t)\varphi_{l,j}(z,t), \qquad T_{h_s}(z,t) = \sum_{j=0}^{M} T_{s,j}(t)\varphi_{s,j}(z,t). \tag{4.8}$$

Letting $T_{l,N}(t) \equiv 0$, $T_{s,0}(t) \equiv 0$ and $T_{s,M}(t) \equiv T_a$ yields approximations $T_{h_l}(z,t)$ and $T_{h_s}(z,t)$ that satisfy the Dirichlet boundary conditions at the interface and at $z = z_b$. The computational problem is to obtain the time-dependent coefficients $T_{l,j}(t)$ for $j = 0, 1, \ldots, N-1$ and $T_{s,j}(t)$ for $j = 1, 2, \ldots, M-1$. Substituting these approximations in the Galerkin forms for T_l and T_s, respectively, and taking the weight functions $v(z,t)$ and $w(z,t)$ to be the hat functions $\varphi_{l,j}$ and $\varphi_{s,j}$, respectively, yields the two systems of equations in matrix form

$$\mathbf{M}_l\frac{d\mathbf{T}_l}{dt} + \mathbf{N}_l\mathbf{T}_l = \mathbf{b}_l, \tag{4.9a}$$

$$\mathbf{M}_s\frac{d\mathbf{T}_s}{dt} + \mathbf{N}_s\mathbf{T}_s = \mathbf{b}_s, \tag{4.9b}$$

where $\mathbf{T}_l = (T_{l,i})$, $\mathbf{M}_l = (M_{l,ij})$, $\mathbf{N}_l = (N_{l,ij})$, $\mathbf{b}_l = \begin{pmatrix} b_l & 0 & \cdots & 0 \end{pmatrix}^T$, $\mathbf{T}_s = (T_{s,i})$, $\mathbf{M}_s = (M_{s,ij})$, $\mathbf{N}_s = (N_{s,ij})$ and $\mathbf{b}_s = (b_{s,i})$.

The nonzero entries of the matrices and the vectors on the right hand side are the following.

$$M_{l,0\,0} = \frac{1}{2}h_l(t), \qquad M_{l,i\,i} = h_l(t) \quad i = 1, \ldots, N-1, \tag{4.10a}$$

$$N_{l,i-1\,i} = -\frac{1}{6}\frac{3i-2}{N}\frac{ds}{dt} - \frac{1}{h_l(t)}, \tag{4.10b}$$

$$N_{l,0\,0} = \frac{1}{6N}\frac{ds}{dt} + \frac{1}{h_l(t)}, \qquad N_{l,i\,i} = \frac{1}{3N}\frac{ds}{dt} + \frac{2}{h_l(t)}, \quad i = 1, \ldots, N-1, \tag{4.10c}$$

$$N_{l,i+1\,i} = \frac{1}{6}\frac{3i+2}{N}\frac{ds}{dt} - \frac{1}{h_l(t)}, \tag{4.10d}$$

$$b_{l,0} = \frac{I}{I_{ref}} \tag{4.10e}$$

$$M_{s,i\,i} = h_s(t), \tag{4.10f}$$

$$N_{s,i-1\,i} = -\frac{1}{6}\frac{3M-3i+2}{M}\frac{ds}{dt} - \frac{1}{h_s(t)} \tag{4.10g}$$

$$N_{s,i\,i} = -\frac{1}{3M}\frac{ds}{dt} + \frac{2}{h_s(t)}, \tag{4.10h}$$

$$N_{s,i+1\,i} = \frac{1}{6}\frac{3M-3i-2}{M}\frac{ds}{dt} - \frac{1}{h_s(t)} \tag{4.10i}$$

$$b_{s,M-1} = T_a\left(\frac{1}{3M}\frac{ds}{dt} + \frac{1}{h_s(t)}\right). \tag{4.10j}$$

On the mass matrices $\mathbf{M}_l$ and $\mathbf{M}_s$ lumping is performed. Note that lumping is $\mathcal{O}(h^2)$ and therefore does not affect the order.

The Stefan condition in (4.1) can be approximated by

$$-\lambda_f \frac{ds}{dt} = \left\{ \sum_{j=0}^{N-1} T_{l,j}(t)\ \frac{\partial \varphi_{l,j}}{\partial z}\bigg|_{z\uparrow s} - \sum_{j=1}^{M-1} T_{s,j}(t)\ \frac{\partial \varphi_{s,j}}{\partial z}\bigg|_{z\downarrow s} \right\}. \tag{4.11}$$

Using the properties of the hat functions this simplifies to

$$\frac{ds}{dt} = \frac{1}{\lambda_f}\left\{ \frac{1}{h_l(t)} T_{l,N-1}(t) + \frac{1}{h_s(t)} T_{s,1}(t) \right\}. \tag{4.12}$$

Thus, the problem (4.1) has been changed to the system of initial-value problems comprising (4.9) and (4.12), with suitable initial conditions. Note that this derivation for two-dimensional problem is not this straightforward because of the Stefan condition.

The discretisation of the time derivatives in (4.9) and (4.12) will be done by the θ-method. We will outline the procedure for Euler forward (EF) for the boundary and a θ-method for the temperature distributions in the following.

Assume the temperature distributions and the position of the solid-liquid interface are known at time level $t = t^k$. We denote these by $\mathbf{T}_l^k$, $\mathbf{T}_s^k$ and s^k, respectively. Here $t^k = k\Delta t$, where Δt is the time step. Then, we compute s^{k+1} through the EF-discretized version of (4.12)

$$s^{k+1} = s^k + \frac{\Delta t}{\lambda_f}\left\{ \frac{1}{h_l(t^k)} T_{l,N-1}^k + \frac{1}{h_s(t^k)} T_{s,1}^k \right\}. \tag{4.13}$$

Now the new mesh can be computed using (4.4) and (4.5). The temperature distributions at time $t = t^{k+1}$ are now computed via the solution of the discretized versions of the matrix equations (4.9).

$$\left(\mathbf{I} + \theta\Delta t \left(\mathbf{M}_l^{k+1}\right)^{-1} \mathbf{N}_l^{k+1}\right) \mathbf{T}_l^{k+1} = \left(\mathbf{I} - (1-\theta)\Delta t \left(\mathbf{M}_l^{k}\right)^{-1} \mathbf{N}_l^{k}\right) \mathbf{T}_l^{k} + \Delta t \left(\theta \left(\mathbf{M}_l^{k+1}\right)^{-1} + (1-\theta)\left(\mathbf{M}_l^{k}\right)^{-1}\right) \mathbf{b}_l \tag{4.14a}$$

and

$$\left(\mathbf{I} + \theta\Delta t \left(\mathbf{M}_s^{k+1}\right)^{-1} \mathbf{N}_s^{k+1}\right) \mathbf{T}_s^{k+1} = \left(\mathbf{I} - (1-\theta)\Delta t \left(\mathbf{M}_s^{k}\right)^{-1} \mathbf{N}_s^{k}\right) \mathbf{T}_s^{k} + \Delta t \left(\theta \left(\mathbf{M}_s^{k+1}\right)^{-1} \mathbf{b}_s^{k+1} + (1-\theta)\left(\mathbf{M}_s^{k}\right)^{-1} \mathbf{b}_s^{k}\right) \tag{4.14b}$$

where the superscripts in the matrix notations denote the time level at which they are evaluated. We know that for $\theta = \frac{1}{2}$ (Crank-Nicolson) the time stepping is $\mathcal{O}(\Delta t^2)$.

4.2 Finding suitable initial conditions

The major problem that remains is to find suitable initial conditions. This problem will be addressed below by looking at the premelting problem.

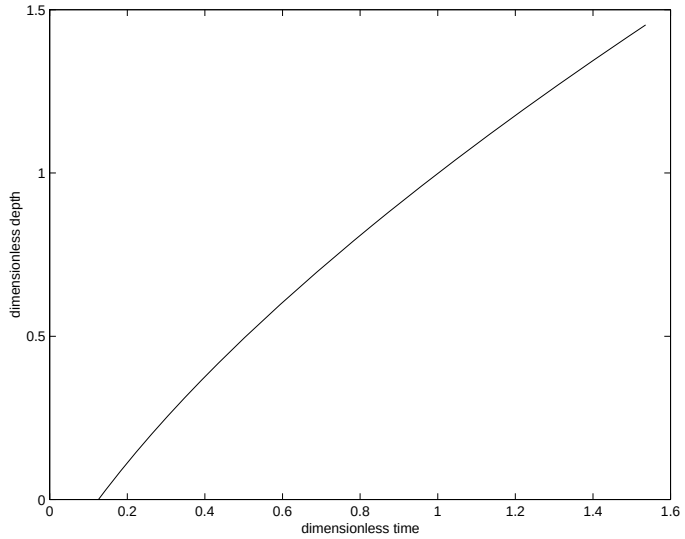

Figure 5: *The position of the solid-liquid interface where the absorption of latent heat is neglected for the case of aluminium.*

In the heating-up stage, the temperature T in the material is governed by

$$\frac{\partial T}{\partial t} = \frac{\partial^2 T}{\partial z^2}, \qquad z > 0. \tag{4.15}$$

The (dimensionless) energy, which we denote by F, is supplied at the surface:

$$\frac{\partial T}{\partial z} = -F, \qquad z = 0, \tag{4.16}$$

and we assume an ambient temperature both at infinity

$$T \to T_a, \qquad z \to \infty, \tag{4.17}$$

as well as initially

$$T = T_a, \qquad t = 0. \tag{4.18}$$

We can find the analytical solution to (4.15)-(4.18) using Laplace transformations. This yields

$$T(z,t) = F\left\{2\left(\frac{t}{\pi}\right)^{\frac{1}{2}} \exp\left(-\frac{z^2}{4t}\right) - z \text{ erfc } \left(\frac{z}{2t^{\frac{1}{2}}}\right)\right\} + T_a. \tag{4.19}$$

Therefore, when latent heat is neglected, the position s of the solid-liquid interface is found from

$$\frac{I}{I_{ref}}\left\{2\left(\frac{t}{\pi}\right)^{\frac{1}{2}} \exp\left(-\frac{s^2}{4t}\right) - s \text{ erfc } \left(\frac{s}{2t^{\frac{1}{2}}}\right)\right\} + \bar{T}_a = 0, \tag{4.20}$$

for all t. In Figure 5 this position is sketched for aluminium. This yields the right initial value of $\frac{ds}{dt}$. From this we compute $s(\Delta t)$ by an EF step. Furthermore, from (4.19) it follows that at time $t = t_m$, with

$$t_m = \frac{I_{ref}^2 T_a^2 \pi}{4I^2}, \tag{4.21}$$

the surface starts to melt.

Now we need initial conditions for the temperature distributions. From the Stefan condition (4.1) it follows that

$$\left.\frac{\partial T_s}{\partial z}\right|_{z\downarrow s} = \lambda_f \frac{ds}{dt} - \left.\frac{\partial T_l}{\partial z}\right|_{z\uparrow s} \approx \lambda_f \frac{ds}{dt} - \frac{I}{I_{ref}}, \tag{4.22}$$

for s small. Therefore we let

$$T_{s,j}(\Delta t) = \\ |T_a| \exp\left(-\frac{(z_{s,j}-s)^2 F^2}{T_a^2 \pi}\right) - F(z_{s,j}-s)\ \mathrm{erfc}\ \left(\frac{(z_{s,j}-s)F}{|T_a|\sqrt{\pi}}\right) + T_a, \qquad j = 1, \ldots, M-1, \tag{4.23}$$

be the initial temperature distribution in the solid at time level $t = \Delta t$ to our computational problem as sketched in Section 4.1, where

$$F = \frac{I}{I_{ref}} - \lambda_f \frac{ds}{dt}. \tag{4.24}$$

Because $s(\Delta t)$ is small, we take the temperature distribution in the liquid at time level $t = \Delta t$ to be linear

$$T_{l,j}(\Delta t) = \frac{I}{I_{ref}}\,(s - z_{l,j})\,, \qquad j = 0, \ldots, N-1 \tag{4.25}$$

satisfying the boundary conditions at $z = 0$ and $z = s$.
Note that this approach cannot easily be extended to cover problems with no constant energy supply.

Now, our numerical method to obtain the depth of the melt pool generated by the laser is solvable.

4.3 Discretisation of the Enthalpy Problem

A discretisation of the enthalpy method in one spatial dimension which uses finite differences is described in Tacke [10]. However, the extension of this model to two spatial dimensions is very hard and becomes even harder when moving boundaries (as in the solidification problem) come up. The finite element method as before looks promising to handle these kinds of problems.

Again, the derivation of the finite element method consists of the following steps: (i) a Galerkin formulation, (ii) a discretizing method and (iii) the solution of the resulting initial value problems with suitable initial conditions.

The problem, to begin with, is comprised by (3.16)-(3.19) and Eq. (3.14) or (3.15). The domain is bounded at $z = z_b$ and we let $\Omega = (0, z_b)$. We search for a weak solution by solving

$$\int_\Omega \frac{\partial H}{\partial t} v dz = D\frac{I}{I_{ref}} v(0) - D\int_\Omega \frac{\partial T}{\partial z}\frac{\partial v}{\partial z} dz, \tag{4.26}$$

together with the relationship between H and T as expressed in Eq. (3.14) or (3.15).

To solve this Galerkin form, we compute approximate solutions of the temperature and enthalpy, from which the position of the solid-liquid interface then follows a posteriori. First we fix the time t and divide the domain $0 \le z \le z_b$ into N subintervals. At each node in this domain we construct the hat function $\varphi_i(z)$. Next we determine approximate solutions of the forms

$$\tilde{H}(z,t) = \sum_{i=0}^{N} H_i(t)\varphi_i(z), \qquad \tilde{T}(z,t) = \sum_{i=0}^{N} T_i(t)\varphi_i(z). \tag{4.27}$$

Letting $H_N(t) \equiv H(\bar{T}_a)$ and $T_N(t) \equiv \bar{T}_a$ takes care of the ambient conditions at $z = z_b$. The computational problem is to obtain the time-dependent coefficients $H_i(t)$ and $T_i(t)$ for $i = 0, \ldots, N-1$. Substituting the approximations into the Galerkin form and taking the weight function $v(z)$ to be the hat functions $\varphi_j(z)$ for $j = 0, \ldots, N-1$, we obtain the set of equations in matrix form:

$$\mathbf{M}\frac{d\mathbf{H}}{dt} = D\mathbf{b} - D\mathbf{N}\mathbf{T}. \tag{4.28}$$

Here, $\mathbf{H} = (H_0(t), \ldots, H_{N-1}(t))^T$ and $\mathbf{T} = (T_0(t), \ldots, T_{N-1}(t))^T$. The entries of the matrices and vector are given by

$$M_{i\,j} = \int_0^{z_b} \varphi_i \varphi_j dz, \qquad i, j = 0, \ldots, N-1, \tag{4.29a}$$

$$b_j = \frac{I}{I_{ref}}\varphi_j(0) - T_a \int_0^{z_b} \frac{d\varphi_N}{dz}\frac{d\varphi_j}{dz} dz, \quad j = 0, \ldots, N-1, \tag{4.29b}$$

$$N_{i\,j} = \int_0^{z_b} \frac{d\varphi_i}{dz}\frac{d\varphi_j}{dz} dz, \qquad i, j = 0, \ldots, N-1. \tag{4.29c}$$

Thus we have a set of initial value problems which, together with the relationship between enthalpy and temperature, can be solved numerically.

In order to show how we solve (4.28) by the θ-method, we rewrite (4.28) as

$$\mathbf{M}\frac{d\mathbf{H}}{dt} = \mathcal{F}(\mathbf{H}, t) := D(\mathbf{b}(t) - \mathbf{N}\mathbf{T}(\mathbf{H})). \tag{4.30}$$

The enthalpy and temperature distributions in the material at time $t = t^{k+1}$ are then computed by the θ-method. We obtain

$$\mathcal{G}(\mathbf{H}^{k+1}) := \mathbf{M}(\mathbf{H}^{k+1} - \mathbf{H}^k) - \Delta t \left(\theta\mathcal{F}(\mathbf{H}^{k+1}, t^{k+1}) + (1-\theta)\mathcal{F}(\mathbf{H}^k, t^k)\right) = \mathbf{0}. \tag{4.31}$$

This system can be solved together with the pointwise relationship of enthalpy and temperature as in (3.14) or (3.15).

For $\theta = 0$ the procedure is simply the following. Compute the enthalpy distribution in the material at time $t = t^{k+1}$ via

$$\mathbf{M}\mathbf{H}^{k+1} = \mathbf{M}\mathbf{H}^k + \Delta t\mathcal{F}(\mathbf{H}^k, t^k), \tag{4.32}$$

and then update the temperature via the inverse relation of (3.14) or (3.15) to get

$$T_i^{k+1} = T(H_i^{k+1}). \tag{4.33}$$

We note that this discretisation converges to the weak solution for ordinary Stefan problems, see e.g. Elliot and Ockendon [5].

Chosing a $\theta \neq 0$ will lead to a system of nonlinear algebraic equations which can be solved by Newton's method. The iteration to obtain the solution at $t = t^{k+1}$ is as follows

$$\begin{cases} \mathbf{H}^{k+1,l} = \mathbf{H}^{k+1,l-1} - (\partial\mathcal{G}(\mathbf{H}^{k+1,l-1}))^{-1}\mathcal{G}(\mathbf{H}^{k+1,l-1}), \quad l = 1, 2, \ldots, \\ \mathbf{H}^{k+1,0} = \mathbf{H}^k. \end{cases} \tag{4.34}$$

Here, the notation $\partial\mathcal{G}(\mathbf{H})$ denotes the Jacobian of $\mathcal{G}(\mathbf{H})$ and is given by

$$\partial\mathcal{G}(\mathbf{H}) = \mathbf{M} + \Delta t\theta D\mathbf{N}\frac{\partial\mathbf{T}}{\partial\mathbf{H}}(\mathbf{H}). \tag{4.35}$$

The iteration in (4.34) is stopped if a given accuracy for the Newton update has been reached.

For the time-stepping method (4.31) we use (4.19) as the initial solution.

5 Extension to 2D

In the various techniques in modelling the melting for the laser percussion drilling process, we encounter several problems. The main problem is that the solidification model is essentially 2D. So our model has to cope with that.

The extension to two spatial dimensions is necessary for solving the solidifcation model. We demonstrate this for the axisymmetric version of our melting model. The geometry for this Stefan problem is sketched in Figure 6.

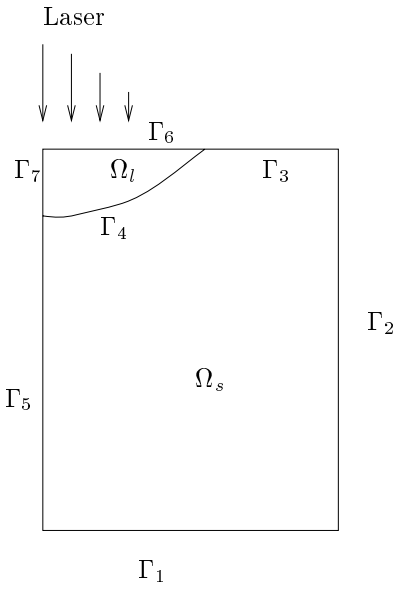

Figure 6: *The geometry for the Stefan formulation.*

The dimensionfull form of the problem is as follows.

$$
\begin{cases}
\rho c \dfrac{\partial T_i}{\partial t} = \operatorname{div}(k \operatorname{grad} T_i), & \text{in } \Omega_i, \quad i = s, l, \\
T_s = T_a, & \text{on } \Gamma_1 \cup \Gamma_2, \\
k \dfrac{\partial T_s}{\partial n} = I(r,t), & \text{on } \Gamma_3, \\
k \dfrac{\partial T_s}{\partial n} = 0, & \text{on } \Gamma_5, \\
k \dfrac{\partial T_l}{\partial n} = I(r,t), & \text{on } \Gamma_6, \\
k \dfrac{\partial T_l}{\partial n} = 0, & \text{on } \Gamma_7, \\
T_s = T_l = T_m, \quad k \dfrac{\partial T}{\partial n}\Big|_l^s = \rho L_f v_n, & \text{on } \Gamma_4.
\end{cases}
\tag{5.1}
$$

Here the normal on Γ_4 points into the solid and v_n is the velocity in normal direction. In this axisymmetric domain the Stefan condition can be rewritten if we denote the position of Γ_4 by

$z = s(r,t)$. The Stefan condition takes the form, see [7],

$$\left[1 + \left(\frac{\partial s}{\partial r}\right)^2\right] \left[k \frac{\partial T}{\partial z}\Big|_l^s\right] = \rho L_f \frac{\partial s}{\partial t}. \tag{5.2}$$

The geometry for the enthalpy method is sketched in Figure 7.

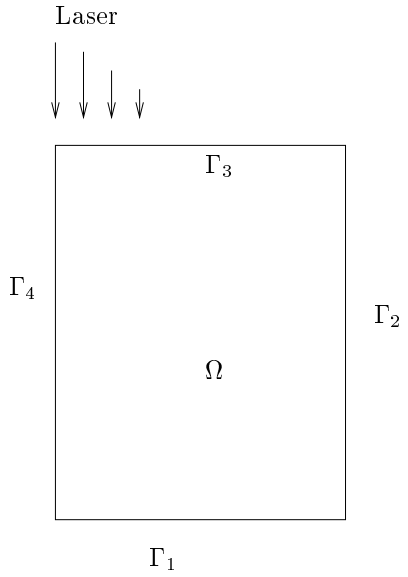

Figure 7: *The geometry for the enthalpy method.*

The dimensionfull form of the problem now reads

$$\begin{cases} \dfrac{\partial H}{\partial t} = \operatorname{div}(k \operatorname{grad} T), & \text{in } \Omega, \\ T = T_a, & \text{on } \Gamma_1 \cup \Gamma_2, \\ k\dfrac{\partial T}{\partial n} = I(r,t), & \text{on } \Gamma_3, \\ k\dfrac{\partial T}{\partial n} = 0, & \text{on } \Gamma_4, \\ T = T_0, & \text{on } t = 0, \end{cases} \tag{5.3}$$

together with the relationship between enthalpy and temperature as described in Eq. (3.14) or (3.15).

The numerical procedure of the 2D Stefan formulation is not straightforward because of the difficult interface condition, whereas the numerics of the 2D enthalpy method is a simple extension of the 1D model. This is mainly because of the fact that in the enthalpy method the position of the solid-liquid interface is not needed. Numerical results of the 2D enthalpy method will be presented and discussed in the next section.

6 Numerical Results and Discussion

In this Section we will discuss the results from the numerical models based on FEM for the melting problem as derived in Sections 4 and 5. The results will be assessed.

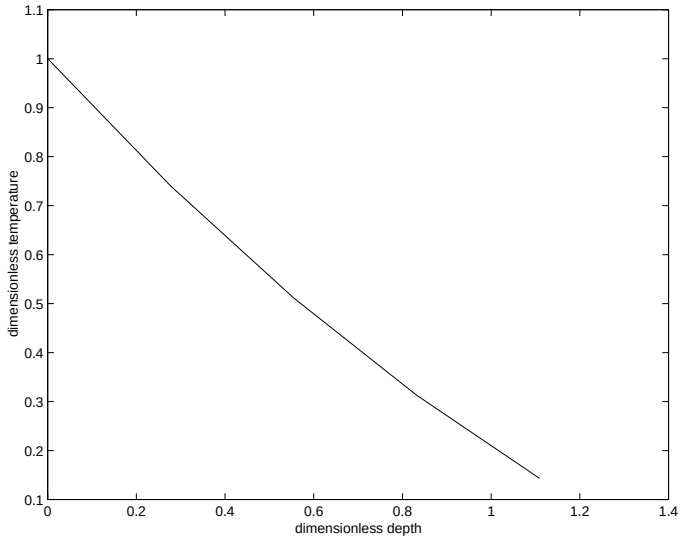

Figure 8: *The temperature distribution in the liquid part at the time at which the surface reaches vaporisation temperature.*

Because Eq. (4.12) is already $O(\Delta t)$, we look at the $O(\Delta t)$ time stepping schemes EF and EB. Note that the results for the (explicit) EF-scheme are obtained using variable time steps to ensure the stability of the scheme. For the Stefan condition method, the $(k+1)$-th time step Δt^{k+1} is taken to be

$$\Delta t^{k+1} = 0.4 \min((h_l(t^k))^2, (h_s(t^k))^2), \tag{6.1}$$

to ensure that the stability condition

$$\Delta t \leq 0.5 h^2 \tag{6.2}$$

holds throughout both regions. Because we need to resolve the temperature in the liquid region h_l will be small and this puts a severe restriction on the time steps used. So if we look at stability, this is in favour of the implicit method. However, for both methods the error is $O(\Delta t) + O(\Delta x^2)$ so to reach the same accuracy we have to take equally small time steps in both methods. In order to get a good estimation for the dimensions of the melt pool, as needed in upcoming splashing and solidification models, we need a high accuracy.

Furthermore, for the explicit method ($\theta = 0$), Eqs (4.14) simplify because of the lumped mass matrices. The matrix in front of $\mathbf{T}_{l,s}^{k+1}$ is simply $\mathbf{I}$. In other words, for this explicit method we do not need to solve a system of equations each time step. The amount of flops to solve a tridiagonal system of n equations is, when one makes use of the sparsity, asymptotically $3n$, see e.g. [4], so here this means an extra amount of calculations of $O(N) + O(M)$. From this we see that the total balance therefore is in favour of using explicit methods after all.

Because the position of the solid-liquid interface is not needed explicitely in the enthalpy method, the restriction on the time step to be used in the enthalpy method is somewhat less severe. The time step Δt (which is constant now) can taken to be

$$\Delta t = 0.4 h^2. \tag{6.3}$$

The results for the EB-scheme for $\Delta t = 0.01$ are shown in Figures 8 to 10. In Figures 8 and 9 the temperatures in the liquid and the solid are shown, respectively, at the time at which the surface reaches vaporisation temperature. Figure 10 shows the evolution of the solid-liquid boundary. Here, the analytical solution in case of latent heat is included as a reference to show its influence.

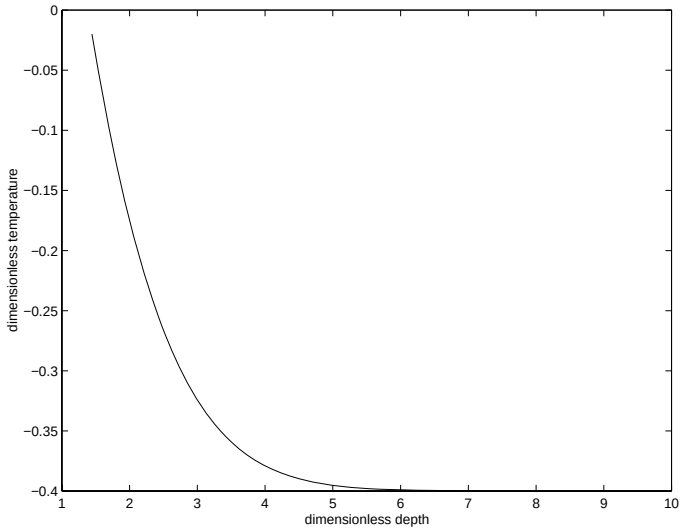

Figure 9: *The temperature distribution in the solid part at the time at which the surface reaches vaporisation temperature.*

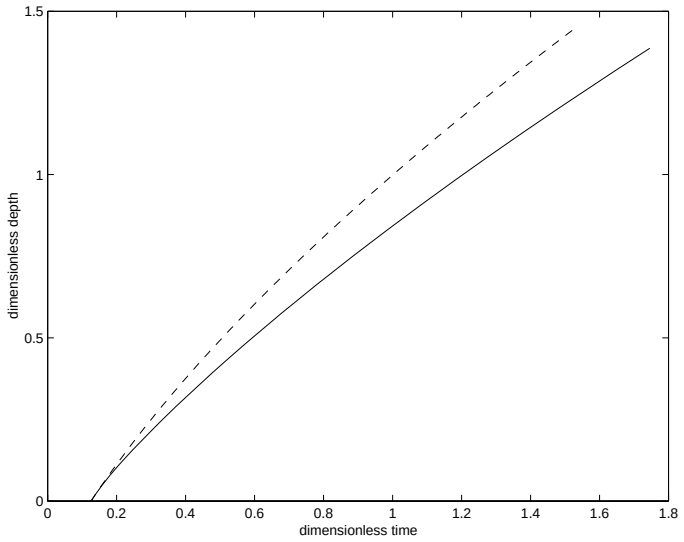

Figure 10: *The position of the solid-liquid interface. The numerical (with latent heat) position is denoted by the solid line, whereas the analytical (without latent heat) position is denoted by the dashed line.*

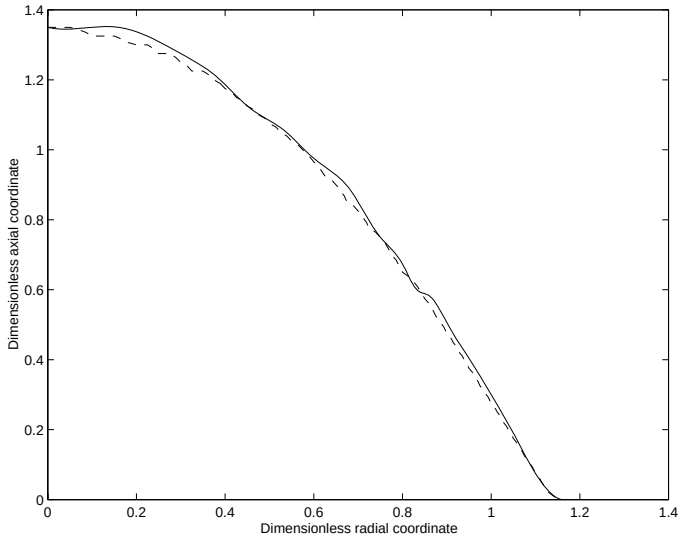

Figure 11: *The front at the time at which the surface in the origin reaches vaporization temperature. The one dimensional result is denoted by the solid line, whereas the result of the full two dimensional model is denoted by the dashed line.*

In Figure 11 the results for the two-dimensional model as derived in the previous section are given compared to the results of the one dimensional analysis. The intensity profile $I(r,t)$ is assumed to be a Gaussian TEM_{00}-mode, constant in time. It is shown that the results for the one-dimensional model indeed give almost identical estimations of the dimensions of the melt pool.

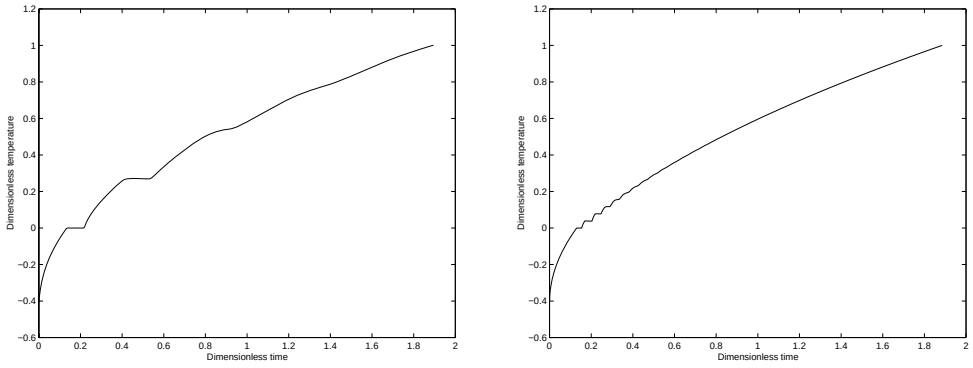

(a) (b)

Figure 12: *Time history plots for temperature in enthalpy problem for (a) 20 elements and (b) for 150.*

If no phase change occurs, the numerics derived from the enthalpy problem are satisfactory. For phase change problems, it is correct on average, since heat balances are fulfilled throughout. However, calculated positions of the solid-liquid interface and temperature and enthalpy oscillate with a period corresponding to the time the interface needs to travel through a certain element. This phenomenon can be seen in Figure 12. The plateau generated propagates to adjacent elements and smoothes out only after the solid-liquid interface has travelled a sufficient distance from the point under consideration.

This staircase-like behaviour has its cause in comparing average enthalpies per element with nodal temperatures. In problems in one spatial dimension this can be overcome by an approach as suggested by Tacke [10]. This method works fairly good, but can't be extended to higher dimensional problems. Another solution is to use a finer grid near the front, the advantage of this is that it is easily extended to higher dimensions. This is an important consideration in view of the splashing and solidification models, see Smith [8].

7 Conclusions and Recommendations

Dimensional analysis shows that radial diffusion on the typical scales can be neglected. A comparison with the two-dimensional model supports this result. Therefore a one-dimensional model predicts the dimensions of the laser induced melt pool accurately.

In this paper two mathematical formulations of laser induced melting have been derived. One formulation uses the Stefan condition whereas the other uses the physical quantity enthalpy.

The implementation of the Stefan condition poses some difficulties. One is that because of the movement of the solid-liquid interface, the domains change in time. Therefore, explicit schemes cause small time steps to ensure that the stability condition holds. In the numerics of the enthalpy method, on the other hand, the domain does not change in time and there is no need to distinguish two different regions. Therefore, the restriction on the time steps is not so severe.

The second difficulty is that choosing suitable initial conditions for the Stefan problem is not straightforward, whereas this is simple for the enthalpy method.

The big advantage of the enthalpy method is that it does not need the position of the solid-liquid interface explicitely in the calculations. This temperature isotherm follows a posteriori. Therefore the enthalpy method is easily extended to 2D. The enthalpy method can thus also be used in the splashing and solidification models as suggested in [8]. In these models some subtleties are involved to deal with convection terms.

Another advantage of the enthalpy method is that it is applicable to situations where alloys are irradiated by a laser. Then we encounter the so called *mushy region*. This is a region where the material is neither solid nor liquid. This region occurs in alloys or glassy substances which do not have a distinct melting point. A model that describes the melting of such a material has to use the enthalpy method, because the Stefan condition needs a distinct melting point. The solidification model breaks down for these kinds of material because the convection in this 'mushy region' is not fully understood, see [8]. Therefore, it is of great importance to see whether (and how) these mushy regions can be approximated by a distinct melting point.

Acknowledgement

The authors wish to acknowledge valuable advise from Pam Byrd and Martien van Dijk. The first author also wishes to acknowledge generous support of Eldim and Rolls Royce to enable him to carry out this research.

References

[1] N.S. Asaithambi. A Galerkin method for Stefan problems. *Appl. Math. Comp.*, 52:239–250, 1992.

[2] J. Crank. *Free and moving boundary problems.* Clarendon Press, 1984.

[3] A.J. Dalhuijsen and A. Segal. Comparison of finite element techniques for solidification problems. *Internat. J. Numer. Methods Engrg.*, 23:1807–1829, 1986.

[4] B.N. Datta. *Numerical linear algebra and applications.* Brooks/Cole, 1995.

[5] C.M. Elliot and J.R. Ockendon. *Weak and variational methods for moving boundary problems.* Research notes in mathematics. Pitman, 1981.

[6] M. Mori. *The finite element method and its applications.* Macmillan publishing company, New York, 1986.

[7] P.D. Patel. Interface conditions in heat-conduction problems with change of phase. *AIAA Journal*, 6:2454, 1968.

[8] W.R. Smith. Models for solidification and spalshing in laser percussion drilling. Rana 00-09, Eindhoven University of Technology, 2000.

[9] J. Stefan. Über die Theorie der Eisbildung, insbesondere über die Eisbildung im Polarmeere. *Annalen der Physik und Chemie*, 42:269, 1891.

[10] K.H. Tacke. Discretization of the explicit enthalpy method for planar phase change. *Internat. J. Numer. Methods Engrg.*, 21:543–554, 1985.

[11] V. Voller and M. Cross. Accurate solutions of moving boundary problems using the enthalpy method. *International Journal of Heat Mass Transfer*, 24:545–556, 1981.

[12] V. Voller and M. Cross. An explicit method to track a moving phase change front. *International Journal of Heat Mass Transfer*, 26:147–150, 1983.

[13] M. Zerroukat and C.R. Chatwin. *Computational Moving Boundary Problems.* Applied and Engineering Mathematics Series 8. John Wiley, New York, 1994.